University of Central Lancashire
UCLan

Central Lancashire Online Knowledge (CLoK)

Title	On the effect of multiple parallel nonlinear absorbers in palliation of torsional response of automotive drivetrain
Type	Article
URL	https://clok.uclan.ac.uk/32128/
DOI	https://doi.org/10.1016/j.ijnonlinmec.2017.06.008
Date	2017
Citation	Harris, A, Motato, E, Mohammad Pour, M, Theodossiades, S, Rahnejat, Homer, O' Mahony, M, Vakakis, A, Bergman, L and McFarland, D (2017) On the effect of multiple parallel nonlinear absorbers in palliation of torsional response of automotive drivetrain. International Journal of Non-Linear Mechanics, 96. pp. 22-35. ISSN 0020-7462
Creators	Harris, A, Motato, E, Mohammad Pour, M, Theodossiades, S, Rahnejat, Homer, O' Mahony, M, Vakakis, A, Bergman, L and McFarland, D

It is advisable to refer to the publisher's version if you intend to cite from the work.
https://doi.org/10.1016/j.ijnonlinmec.2017.06.008

For information about Research at UCLan please go to http://www.uclan.ac.uk/research/

All outputs in CLoK are protected by Intellectual Property Rights law, including Copyright law. Copyright, IPR and Moral Rights for the works on this site are retained by the individual authors and/or other copyright owners. Terms and conditions for use of this material are defined in the http://clok.uclan.ac.uk/policies/

International Journal of Non-Linear Mechanics 96 (2017) 22–35

Contents lists available at ScienceDirect

International Journal of Non-Linear Mechanics

journal homepage: www.elsevier.com/locate/nlm

On the effect of multiple parallel nonlinear absorbers in palliation of torsional response of automotive drivetrain

A. Haris [a], E. Motato [a], M. Mohammadpour [a], S. Theodossiades [a,*], H. Rahnejat [a], M. O' Mahony [b], A.F. Vakakis [c], L.A. Bergman [d], D.M. McFarland [d]

[a] Wolfson School of Mechanical, Electrical and Manufacturing Engineering, Loughborough University, United Kingdom
[b] Ford Motor Company Ltd, Dunton Technical Centre, Laindon, Basildon, Essex, United Kingdom
[c] Department of Mechanical Science and Engineering, University of Illinois at Urbana–Champaign, USA
[d] Department of Aerospace Engineering, University of Illinois at Urbana–Champaign, USA

ARTICLE INFO

Keywords:
Automotive drivetrain
Targeted Energy Transfer
Nonlinear Energy Sink
Frequency–Energy Plot

ABSTRACT

Torsional vibrations transmitted from the engine to the drivetrain system induce a plethora of noise, vibration and harshness (NVH) concerns, such a transmission gear rattle and clutch in-cycle vibration, to name but a few. The main elements of these oscillations are variations in the inertial imbalance and the constituents of combustion power torque, collectively referred to as engine order vibration. To attenuate the effect of these transmitted vibrations and their oscillatory effects in the drive train system, a host of palliative measures are employed in practice, such as clutch pre-dampers, slipping discs, dual mass flywheel and others, all of which operate effectively over a narrow band of frequencies and have various unintended repercussions. These include increased powertrain inertia, installation package space and cost. This paper presents a numerical study of the use of multiple Nonlinear Energy Sinks (NES) as a means of attenuating the torsional oscillations for an extended frequency range and under transient vehicle manoeuvres. Frequency–Energy Plots (FEP) are used to obtain the nonlinear absorber parameters for multiple NES coupled in parallel to the clutch disc of a typical drivetrain configuration. The results obtained show significant reduction in the oscillations of the transmission input shaft, effective over a broad range of response frequencies. It is also noted that the targeted reduction of the acceleration amplitude of the input shaft requires significantly lower NES inertia, compared with the existing palliative measures.

© 2017 The Authors. Published by Elsevier Ltd. This is an open access article under the CC BY license (http://creativecommons.org/licenses/by/4.0/).

1. Introduction

Attenuation of torsional oscillations in automotive powertrains has recently received increased attention owing to a plethora of noise, vibration and harshness (NVH) concerns. These include clutch in-cycle vibration referred to in industry as "whoop" [1–3] and transmission rattle [4–7]. The underlying cause of these phenomena is the transmitted engine order harmonics [8] to the clutch and transmission systems, which are exacerbated through the modern high output power-to-light weight ratio concept, driven by the key objective of fuel efficiency. Light weight components are subjected to flexible structural dynamics, exacerbated by increased power torque fluctuations as the result of enhanced power, particularly with diesel engines. Furthermore, downsized engines with fewer cylinders and lower operating speeds exhibit increased torsional oscillations produced by discrete torque pulses through combustion process and cyclic inertial variation [9,10]. Other new technologies such as stop–start or cylinder deactivation, also developed for improved fuel efficiency and reduced emissions, cause transient intermittency which also leads to the generation of drivetrain vibration [11].

To mitigate the emergent NVH concerns, various palliative measures have been developed, including tuned vibration absorbers such as clutch pre-dampers, the Dual Mass Flywheel (DMF) [12,13] and DMF with Centrifugal Pendulum Vibration Absorbers (CPVA) [14,15]. Numerous studies have reported on the working principle of DMF and its design, including studies of DMF with: radial springs [16], Magneto-Rheological (MR) dampers and arc helix springs [17]. These are primarily meant to mitigate transmission gear rattle. For clutch in-cycle vibration, a Diehl-fix which is essentially a lumped mass-damper is attached to the clutch lever of a mechanical-type clutch [18]. These palliative measures are

* Corresponding author.
E-mail address: S.Theodossiades@lboro.ac.uk (S. Theodossiades).

http://dx.doi.org/10.1016/j.ijnonlinmec.2017.06.008
Received 17 January 2017; Received in revised form 24 May 2017; Accepted 11 June 2017
Available online 20 July 2017
0020-7462/© 2017 The Authors. Published by Elsevier Ltd. This is an open access article under the CC BY license (http://creativecommons.org/licenses/by/4.0/).

Nomenclature

A	Acceleration
C_d	Aerodynamic drag coefficient
c_1, c_2	Damping coefficient
F	Frequency Coefficient of rolling resistance
f_2	Speed dependent coefficient of rolling resistance
F_z	Normal load
J_2, J_3, J_N	Component inertia
k_2, k_3, k_N	Stiffness
r_w	Wheel radius
S	Vehicle frontal area
T_{RES}	Resistance torque
V	Vehicle longitudinal velocity
Z	Modal damping ratio matrix

Greek Symbols

ζ	Damping ratio
θ	Angular motion
ρ	Air density
Φ	Modal matrix
ω	Natural frequency

Abbreviations

AEAAR	Area of Effective Acceleration Amplitude Reduction
CPVA	Centrifugal Pendulum Vibration Absorber
CWT	Continuous Wavelet Transform
EO	Engine Order
FEP	Frequency-Energy Plot
FWD	Front Wheel Drive
LNM	Linear Normal Mode
NNM	Nonlinear Normal Mode
PSD	Power Spectral Density
SMF	Solid Mass Flywheel

invariably costly, only effective over a narrow band of frequencies and add to the mass of the powertrain system as well as increase the package space [19]. Furthermore, these devices are tuned to counteract/filter out some specific range of frequencies. Thus, they exclude the broad band response of internal combustion engines, which aside from the usual engine order (EO) vibrations include elastodynamic responses due to the increasing use of components of low elastic moduli [20] as well as broad band powertrain response to impulsive actions [21–23].

Therefore, there is a need for vibration absorbers which would act over a broader range of frequencies with limited prior tuning. The Nonlinear Energy Sinks (NES) are passive absorbers which operate on the principle of Targeted Energy Transfer (TET). The energy of mechanical vibrations is transferred, in a nearly irreversible manner, from its source (usually a linear primary system) to a recipient (a secondary system; NES), where it is either absorbed, redistributed or dissipated [24].

Vakakis et al. [25] and Gendelman et al. [26] have studied TET in two- and three-degree-of-freedom engineering systems. These were impulsively excited. It was concluded that 1:1 stable sub-harmonic orbits are responsible for energy transfer. Vakakis et al. [27] studied the activation of Nonlinear Normal Modes (NNMs) to describe the interaction of nonlinear absorbers with linear primary systems. Jiang et al. [28] studied, theoretically and experimentally, the steady state passive nonlinear energy pumping in coupled oscillators. Panagopoulos et al. [29] examined the transient resonant interactions of finite linear chains, coupled with an essentially nonlinear attachment. The study presented an alternative approach, allowing simultaneous resonant interactions between the NNMs of the nonlinear absorber and the normal modes of the linear system. McFarland et al. [30] conducted experimental studies of nonlinear energy pumping occurring at a single fast frequency. Kerschen et al. [31] performed studies on linear systems coupled with grounded and ungrounded nonlinear attachments to understand the dynamics of the individual absorbers and their effectiveness. It was highlighted that for both attachments the energy pumping is governed through 1:1 resonance captures. However, the grounded attachments do have limitations in application in certain fields due to the required stiffness and weight.

There have also been studies with regard to the use of different types of stiffness nonlinearity (e.g. non-smooth and non-polynomial [32,33]). Similarly, studies have been conducted on primary systems, coupled to multiple nonlinear attachments, where it was reported that the efficiency of energy transfer is substantially improved when compared with single attachments [34,35]. The above-mentioned studies were conducted on translational systems subject to transient excitations, where it was demonstrated that NES can engage in the suppression of broad band vibration responses.

A dearth of studies exists concerning applications of rotational NES which are necessary to attenuate powertrain NVH concerns which are largely of torsional oscillatory nature, such as gear rattle. In this regard, Viguie et al. [36] examined the implementation of NES to stabilise drill-string systems. The study mainly focused on friction-induced vibrations, which is similar to another clutch NVH phenomenon, referred to as take-up judder [37–39] caused by stick–slip friction of the lining material during clutch engagement. Viguie et al. [36] observed that the NES is able to eliminate limit cycle instabilities. Therefore, their findings can apply to problems such as clutch take-up judder. There are potential applications for NES in tackling a variety of vehicular powertrain NVH issues, which as yet remains untapped.

Recently, Haris et al. [40] showed that nonlinear vibration absorbers can be effective in attenuating torsional vibrations of vehicular driveline system over a broader range of frequencies. However, it was also shown that the efficiency of the NES is highly dependent on the amplitude and frequency of the applied input under various engine transient manoeuvres. Thus, a single NES may not be sufficient to act across the whole spectrum of excitation frequencies.

The majority of studies presented in the literature in the subject area of Targeted Energy Transfer are concerned with the incorporation of nonlinear vibration absorbers (NES) to reduce vibrations in translational systems, with the exception of a few studies only analysing the performance of rotational systems equipped with NES. To the best knowledge of the authors no previous attempt has been made on examining the potential of incorporating (multiple parallel) rotational NES(s) to attenuate torsional vibrations in automotive drivelines. Thus, the implementation of multiple parallel NES to attenuate the broad spectrum of encountered torsional NVH phenomena is the subject of the current study. The driveline system considered is a Front Wheel Drive (FWD) transaxle configuration, powered by a three-cylinder engine. A reduced order drivetrain model is developed and validated both in temporal and spectral domains against measured response of the vehicle under test conditions. Then, the model is modified to incorporate multiple parallel NES. Significant vibration attenuation at the dominant Engine Orders (EO) is noted.

2. The drivetrain model

A transaxle FWD powertrain system with a 3-cylinder engine with a Solid Mass Flywheel (SMF) is considered in the current study. It incorporates a 5-speed manual transmission and a clutch equipped with a clutch pre-damper. A two-degree-of-freedom linear model is used to represent the drivetrain system, comprising the clutch assembly, the transmission, differential and the axle half-shafts (Fig. 1).

The clutch assembly has the inertia J_2, coupled to the transmission input shaft with the inertia J_3. The engine is not included in the model, but the measured oscillatory motion of the flywheel is used as an input

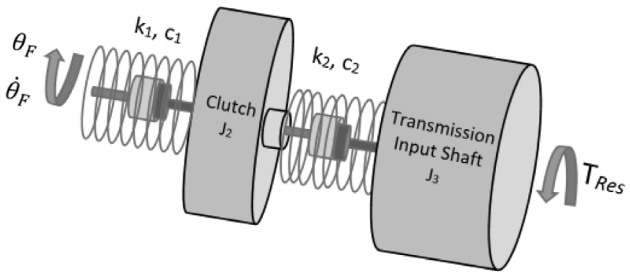

Fig. 1. Schematic representation of the drivetrain model.

Table 1
Typical range of the drivetrain model parameters.

Inertia (kgm^2)	Stiffness (Nm/rad)
J_2 = 0.0005 –0.005	k_1 = 500–5000
J_3 = 0.001 –0.006	k_2 = 5000–30000

to the clutch assembly, denoted by θ_F and $\dot{\theta}_F$. The effect of the other drivetrain components connected to the transmission input shaft J_3 is represented by the resisting torque T_{Res}. The equations of motion become:

$$\begin{bmatrix} J_2 & 0 \\ 0 & J_3 \end{bmatrix} \begin{bmatrix} \ddot{\theta}_2 \\ \ddot{\theta}_3 \end{bmatrix} + [\boldsymbol{C}] \begin{bmatrix} \dot{\theta}_2 \\ \dot{\theta}_3 \end{bmatrix} + \begin{bmatrix} k_2 + k_1 & -k_2 \\ -k_2 & k_2 \end{bmatrix} \begin{bmatrix} \theta_2 \\ \theta_3 \end{bmatrix} = \begin{bmatrix} k_1\theta_F + c_1\dot{\theta}_F \\ -T_{Res} \end{bmatrix} \quad (1)$$

where, θ_2 and θ_3 are the angular displacements of the clutch and the transmission input shaft, respectively. k_1 and k_2 represent the torsional rigidity, connecting the engine to the clutch and the latter to the transmission. $k_1\theta_F + c_1\dot{\theta}_F$ is the input torque applied to the clutch assembly, which is a function of the flywheel motion. Table 1 lists a typical range of parametric values.

The resisting torque T_{Res} [41] is modelled as a function of the tyre rolling resistance T_R, and the aerodynamic drag torque $T_A$as :

$$T_R = \left(f_0 + f_2 V^2\right) F_z r_w \quad (2)$$

$$T_A = \frac{1}{2}\rho S C_d V^2 r_w \quad (3)$$

$$T_{Res} = T_R + T_A \quad (4)$$

where:

F_z is the tyre normal load; f_0 is the coefficient of rolling resistance; f_2 is the speed-dependent coefficient of rolling resistance; r_w is the tyre radius; ρ is the density of air; S is the vehicle frontal area; C_d is the aerodynamic drag coefficient and V is the vehicle longitudinal velocity.

The damping matrix $[\boldsymbol{C}]$ is determined as [42]:

$$[\boldsymbol{C}] = [\boldsymbol{J}][\boldsymbol{\Phi}][\boldsymbol{Z}][\boldsymbol{\Phi}]^T[\boldsymbol{J}] \quad (5)$$

where, $\boldsymbol{\Phi}$ is the modal matrix obtained through solution of the generalised eigenvalue problem and **Z** is the diagonal modal damping ratio matrix:

$$[\boldsymbol{Z}] = \begin{bmatrix} 2\zeta_1\omega_1 & 0 \\ 0 & 2\zeta_2\omega_2 \end{bmatrix} \quad (6)$$

where, ζ_i is the damping ratio of the "ith" mode, corresponding to modal natural frequency; ω_i.

Solution of Eqs. (1)–(6) provides the drivetrain response. The predictions of the model are compared with experimental measurements obtained from the test vehicle. The experimental data is acquired through use of sensors mounted onto the flywheel and the transmission input shaft, measuring their angular velocities. Variable sampling rate was used, as the sensors were programmed to register the passage of the reflective surface patches (at each revolution) mounted on both the flywheel and the transmission input shaft. The test manoeuvre corresponds to the 1st gear engaged at 100% throttle input over the entire engine operating range with the total test duration of 5s.

Table 2
Tuned modal damping ratios and natural frequencies.

Damping ratio	Natural frequency (Hz)
ζ_1 = 0.8	ω_1 = 60
ζ_2 = 0.5	ω_2 = 800

The modal damping ratios are optimised so that the model response is bounded and in good agreement with the experimental data. Table 2 lists the tuned modal damping ratios and the corresponding natural frequencies. The resultant damping ratios are high due to the fact that the vehicle driveline considered is equipped with torsional dampers.

Model validation is performed in both spectral and temporal domains. Spectral analysis is carried out, using Morlet-based Continuous Wavelet Transform (CWT) in order to capture the transient frequency content at the various EO contributions. The CWT plots highlight the presence of several EO harmonics with the 1.5 EO being the most significant for a 3-cylinder 4-stroke engine with no cylinder-to-cylinder or cycle-to-cycle combustion variations [8]. This is because combustion takes place three times over two successive crankshaft revolutions. The CWT plots in Fig. 2 show a comparison between the experimentally measured and numerically predicted responses of the transmission input shaft velocity. Good agreement is noted. The response in the time domain presented in Fig. 3 also demonstrates good correlation between the experimental and the numerical results, with the insets to the figure showing the corresponding CWT plots at different engine speeds.

The validation exercise is performed for different manoeuvres. An example of the time domain response of the transmission input shaft with the 3rd gear engaged at 25% throttle is shown in Fig. 4, where again good correlation is observed between the numerical and experimental results.

3. Drivetrain model equipped with a single NES

The drivetrain model is then modified to incorporate a single NES mounted in parallel to the clutch friction disc, as shown in Fig. 5. The NES has a cubic restoring force coefficient and is classified as an ungrounded attachment. As the studied application is an automotive drivetrain, where the rigid body motion of the system cannot be physically eliminated, the grounded attachment is not a realisable option. A manoeuvre in 1st gear at 25% throttle is used to analyse the performance of the NES through the entire engine speed range. This manoeuvre is chosen because of its lower input power content (thus, lower energy content to engage the NES with the primary system) compared with those at higher throttle levels. The matrix formulation describing the drivetrain dynamics with an attached NES becomes:

$$\begin{bmatrix} J_2 & 0 & 0 \\ 0 & J_3 & 0 \\ 0 & 0 & J_N \end{bmatrix} \begin{bmatrix} \ddot{\theta}_2 \\ \ddot{\theta}_3 \\ \ddot{\theta}_N \end{bmatrix} + [\boldsymbol{C_N}] \begin{bmatrix} \dot{\theta}_2 \\ \dot{\theta}_3 \\ \dot{\theta}_N \end{bmatrix} + \begin{bmatrix} k_2 + k_1 & -k_2 & 0 \\ -k_2 & k_2 & 0 \\ 0 & 0 & 0 \end{bmatrix} \begin{bmatrix} \theta_2 \\ \theta_3 \\ \theta_N \end{bmatrix} = \begin{bmatrix} k_1\theta_F + c_1\dot{\theta}_F - k_N\left(\theta_2 - \theta_N\right)^3 \\ -T_{Res} \\ k_N\left(\theta_2 - \theta_N\right)^3 \end{bmatrix} \quad (7)$$

where, J_N, k_N *and* θ_N are the inertia, nonlinear stiffness and angular displacement of the NES.

To evaluate the effectiveness of the NES, the performance of the system with *active* NES is compared with that of the system with a *locked* NES. The latter is essentially a system, where the NES inertia is simply added to the inertia of the clutch disc. The reason is that the addition of some inertia to the system is expected to lead to vibration attenuation to a certain extent anyway. This approach has been widely followed in the relevant TET literature [35,43,44].

The matrix formulation for the *locked* NES becomes:

$$\begin{bmatrix} J_2 + J_N & 0 \\ 0 & J_3 \end{bmatrix} \begin{bmatrix} \ddot{\theta}_2 \\ \ddot{\theta}_3 \end{bmatrix} + [\boldsymbol{C}] \begin{bmatrix} \dot{\theta}_2 \\ \dot{\theta}_3 \end{bmatrix} + \begin{bmatrix} k_2 + k_1 & -k_2 \\ -k_2 & k_2 \end{bmatrix} \begin{bmatrix} \theta_2 \\ \theta_3 \end{bmatrix} = \begin{bmatrix} k_1\theta_F + c_1\dot{\theta}_F \\ -T_{Res} \end{bmatrix}. \quad (8)$$

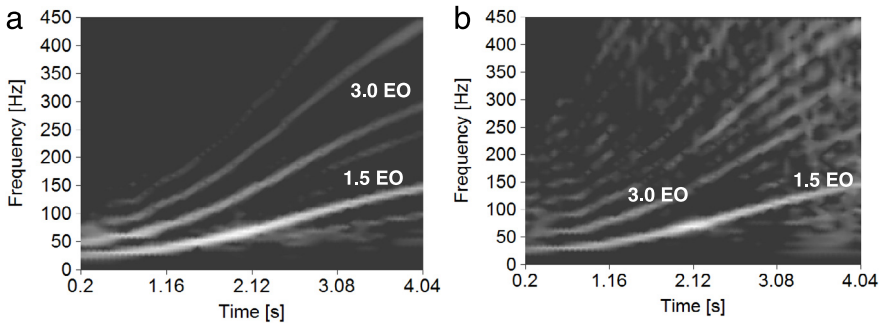

Fig. 2. a) CWT of the numerical predictions and b) CWT of the experimental measurements (1st gear engaged at 100% throttle).

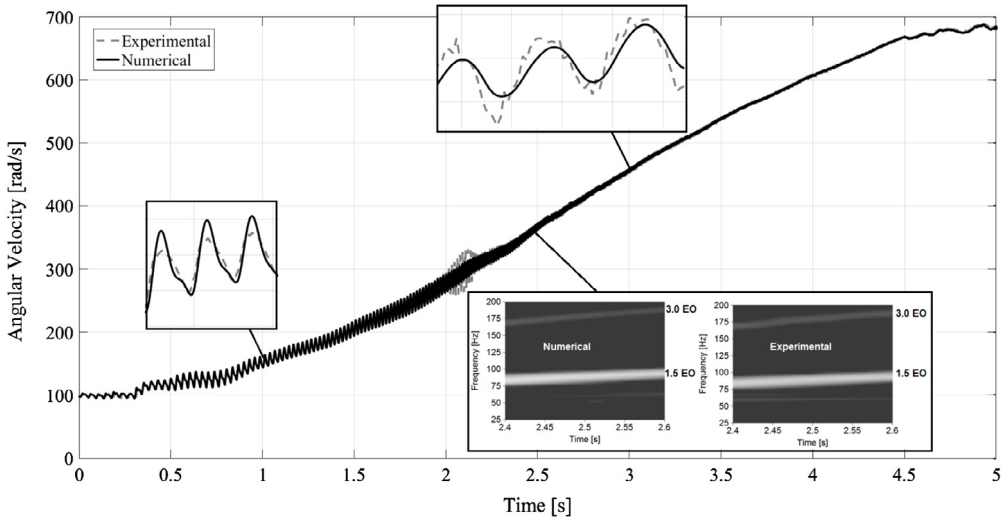

Fig. 3. Numerical and experimental time histories of the transmission input shaft velocity and CWT insets (1st gear engaged at 100% throttle).

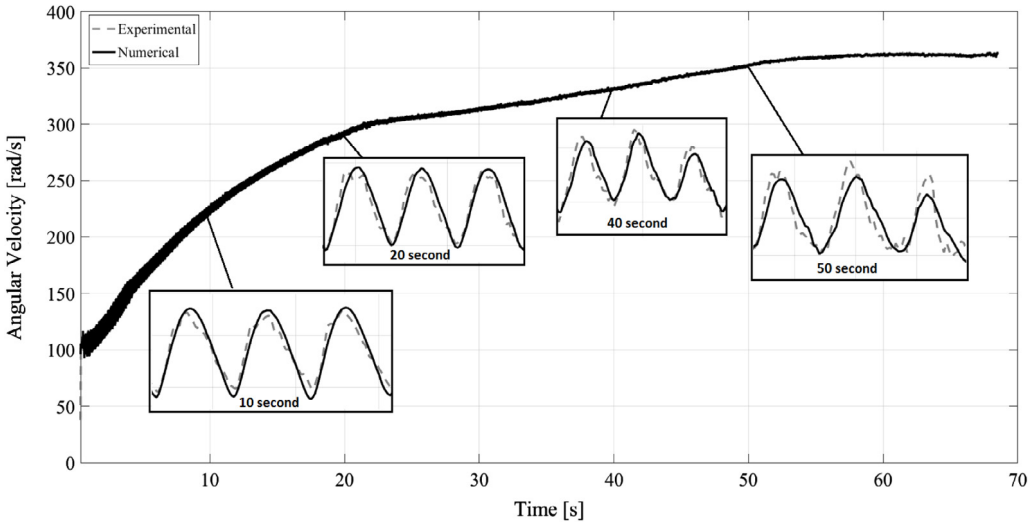

Fig. 4. Numerical and experimental time histories of the transmission input shaft velocity (3rd gear engaged at 25% throttle).

The damping matrix $[\boldsymbol{C_N}]$ in Eq. (7) is formed by adding the corresponding NES damping coefficient to the damping matrix $[\boldsymbol{C}]$ of the *locked* NES model using the approach in [42], thus:

$$[\boldsymbol{C_N}] = \begin{bmatrix} c_{(1,1)} & c_{(1,2)} & -c_N \\ c_{(2,1)} & c_{(2,2)} & 0 \\ -c_N & 0 & c_N \end{bmatrix} \tag{9}$$

where, c_N is the damping coefficient of the NES and $c_{(i,j)}$ is the damping coefficient of the linear drivetrain model with a *locked* NES.

The NES performance is evaluated through comparison of the spectral contribution at 1.5 EO to the overall acceleration amplitude of the transmission input shaft for both the *locked* and the *active* NES systems. The reason for selecting this metric as the main performance index is that the 1.5 EO is the fundamental firing order of the 3-cylinder

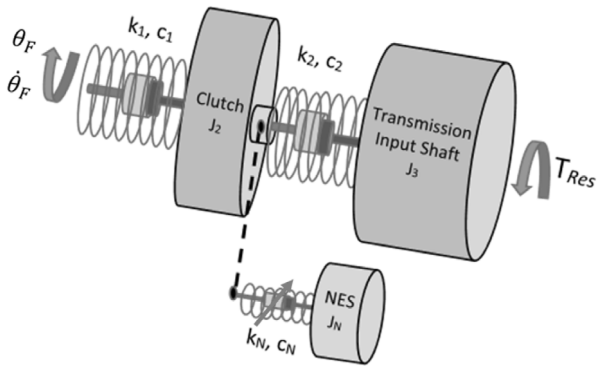

Fig. 5. Schematic representation of drivetrain equipped with a single NES.

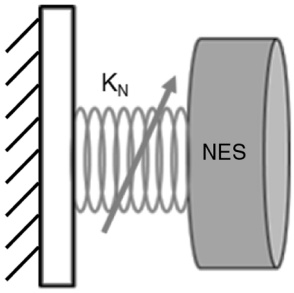

Fig. 6. The single degree of freedom grounded NES used to produce the FEP.

engine. Therefore, the generated torsional vibrations are expected to have higher severity at this particular frequency. By comparing the 1.5 EO acceleration amplitudes it is possible to assess the frequency region where the NES provides some vibration attenuation. It should be noted that the NES is not a frequency-tuned absorber. Instead it functions as an input energy-dependent absorber. Essentially nonlinear absorbers have the feature to exhibit energy threshold values, which define the boundary between efficient and inefficient vibration reduction. Therefore, the design of nonlinear absorbers is based on the input energy instead of the excitation frequency. An NES which is deemed to suppress vibrations in a specific frequency range would work in all scenarios provided that the energy supplied is above its effective operation threshold [45].

The Matlab command *Pwelch* is used to obtain the acceleration amplitudes corresponding to the 1.5 EO harmonics as the model is created in the Matlab/Simulink environment. This command calculates the Power Spectral Density (PSD) of the input signal using Welch's overlapped segment-averaging estimator. The acceleration signal of the transmission input shaft obtained from the numerical model is provided as the input to *Pwelch*, which returns the PSD with units of $rad^2/s^4/Hz$. The resultant PSD is processed as $\sqrt{PSD \times 1.5EOFrequency}$, where the nominated frequency is the 1.5 EO harmonic.

Before conducting thorough numerical simulations to determine the effective characteristics of the NES, suitable ranges for the restoring force coefficient and NES inertia are identified. This is accomplished by analysing the FEP of a single degree of freedom grounded NES attachment, as shown in Fig. 6. The FEP is a graphical representation of the NNMs (which are defined as free periodic and synchronous oscillations of the undamped, unforced system [46]), where the amplitude of an NNM is plotted with respect to its energy content. Each point on the FEP signifies an NNM motion at a frequency corresponding to the periodic motion and at an energy level equal to the conserved total energy [46].

The numerical computation of the NNMs is performed using a Matlab code developed by Peeters et al. [47]. The code utilises combination of shooting and pseudo-arc length continuation methods for computing the NNM motions. The algorithm is initiated at the low energy Linear Normal Mode (LNM) and uses a predictor step between two NNM motions at different energy levels. Then, the corrector step is used to refine the predictions in order to obtain the actual solution at a specific energy level. In order to compute the NNMs, the algorithm requires input parameters defining the nature of the oscillatory system, such as the linear stiffness, inertia/mass, restoring force coefficients and the order of the nonlinearity (e.g. cubic). Additionally, if the initial conditions are known *a priori,* then these can be provided as an input to the algorithm. Usually, this is the initial displacement of the system corresponding to an equilibrium condition (zero velocity).

The NNMs of the system depicted in Fig. 6 are computed and shown in Fig. 7. This plot comprises three backbone curves, superimposed on the wavelet of the drivetrain model equipped with an NES. The backbone curves are the FEPs of the single degree of freedom grounded NES, whereas the wavelet represents the total energy of the drivetrain model with an NES attachment for a manoeuvre in 1st gear at 25% throttle, computed using:

$$E_{Total} = \sum K_E + \sum P_E \tag{10}$$

where, K_E is the kinetic energy and P_E the potential energy of the drivetrain model equipped with an NES:

$$\sum K_E = \sum \frac{1}{2} J_i \dot{\theta}_i^2 \tag{11}$$

$$\sum P_E = \sum \frac{1}{2} k_i \theta_i^2 + \frac{1}{4} k_N \theta_N^4 \tag{12}$$

where $i = 2\,(clutch), 3\,(transmission\ input\ shaft), N\,(NES)$.

Each backbone curve represents the NNM motion of the grounded NES with a given inertia and restoring force coefficient. As the frequency increases with the energy level, the system exhibits hardening characteristics. The conclusion drawn from the FEP is that the NES would be expected to work effectively in the frequency regions, where the FEP curves cross the system energy (i.e. wavelet). Therefore, as it can be seen in Fig. 7, there is a possibility to target higher or lower frequency regions, depending on the parameters of NES design. In order to put this into context, an NES with parameters J_N = *7% of the transmission input shaft inertia,* $k_N = 5 \times 10^5$ *Nm/rad*^{3} and damping coefficient c_N = *0.001 Nms/rad* is chosen. The plot of the 1.5 EO acceleration amplitude response of the transmission input shaft with *locked* and *active* NES is shown in Fig. 8.

Fig. 8 shows that the NES with the above parameters attenuates the vibrations over a broad frequency range (80–140 Hz), which correlates with that predicted by the FEP in Fig. 7 (circled). The reason for the suppression of vibrations in this range is that the energy of the powertrain system (1st gear with 25% throttle) is within the operating threshold of the NES, thus the overlap of the NNMs with the wavelet content. It should be noted that the effectiveness of the NES depends on the input energy of the system. The frequency range here is only used as a criterion to assess the ability of NES to attenuate vibration, which by no means makes the NES a frequency-dependent absorber.

According to the FEPs in Fig. 7, if attenuation of vibration is required at lower frequencies, an NES with lower restoring force coefficient should be chosen. On the other hand, for attenuation at higher frequencies, an NES with higher restoring force coefficient would be required. It is important to note that the above configuration may not always be sufficient, as the NES effectiveness depends on the supplied input energy. Moreover, for NESs with given nonlinear stiffness and varying inertia, the frequency range where vibration attenuation is achieved would also vary. This behaviour is highlighted by the two higher frequency FEPs in Fig. 7. Finally, it is noteworthy that if the system presented in Fig. 6 was linear, the backbone curve of Fig. 7 would only comprise a horizontal line, corresponding to the natural frequency of the system (since it does not depend on the energy input).

The effect of lower restoring force coefficient on the NES performance is shown in Fig. 9. There is a noticeable difference in the system energy fluctuations (wavelet) coupled with an NES tuned at lower

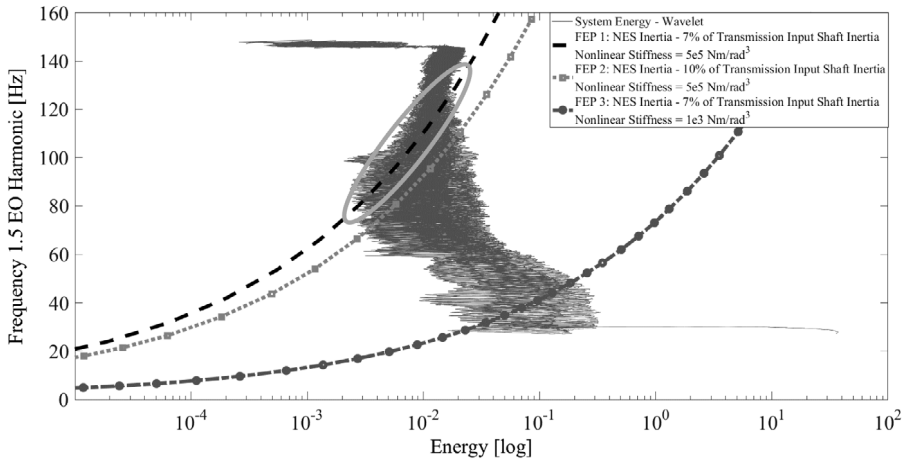

Fig. 7. FEP of the single-degree-of-freedom grounded NES and energy wavelet of the drivetrain model equipped with a single NES (1st gear engaged at 25% throttle).

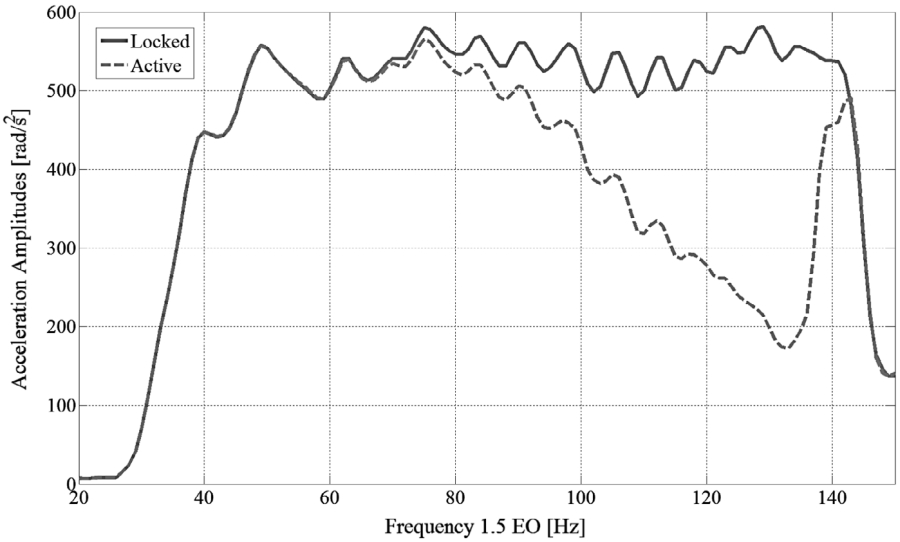

Fig. 8. Acceleration amplitude of the 1.5 EO at the transmission input shaft 1st gear engaged at 25% throttle) for a drivetrain equipped with a single NES (J_N = 7% of the transmission input shaft inertia, k_N = 5 x 10^5 Nm/rad^3, c_N = 0.001 Nms/rad).

frequencies (Fig. 9), when compared with a system coupled with an NES tuned at higher frequencies (Fig. 7). In the case of the latter, the system energy is localised in a continuous single frequency range (20–140 Hz). Conversely, Fig. 9 shows that the energy content of the wavelet is spread into three different frequency regions (20–80 Hz), (80 –120 Hz) and (120–150 Hz). In the first region (i.e. 20–80 Hz), the system energy is centralised around a particular energy level (10^{-1}). In this case the inclusion of the NES has led to a redistribution of the system energy in the higher frequency region (i.e. 80 –150 Hz), where there is a significant amount of energy available; 10^{-4} – 10^{-2}. This phenomenon shows how an NES can induce energy redistribution in the primary system by transferring the oscillatory energy from low to high frequency regions, where it can be dissipated through structural damping [48]. The rubber-mass damper, known as the Diehl-fix, attached to the clutch-lever of mechanical clutches in some vehicles essentially acts in the same manner by shifting the energy level from the natural frequency of the lever to higher frequencies, but is tuned for the purpose unlike the NES [2,3].

To evaluate the FEP predictions at low frequencies, the acceleration response amplitude of the transmission input shaft, equipped with *locked* and *active* NES are produced and shown in Fig. 10. The NES parameters are J_N = *8% of the transmission input shaft inertia,* k_N = 1×10^4 *Nm/rad*^{3} with a damping coefficient of c_N = *0.001 Nms/rad*). The frequency region: 60–80 Hz, where vibration attenuation is observed correlates well with the predictions of the FEP (the circled region in Fig. 9).

Hitherto, the NES parameters have been chosen using the FEPs. Generally, the weight/inertia of the absorber is crucial in the overall performance of the system and for automotive applications it should be kept as light and compact as possible. The range of the NES parameters are selected in order to attenuate vibrations at higher frequencies: the inertia range between *8-15%* of the transmission input shaft inertia and the restoring force coefficient in the range: $k_N = 1\times10^4 - 1\times10^7$ *Nm/rad*^{3} are instructive. The NES damping coefficient is chosen as: c_N = *0.001 Nms/rad* for as low an attenuation of the absorber's response as possible.

Reduced transmission input shaft angular acceleration amplitudes below 200 rad/s^2 have been reported for engine speeds exceeding 800 rpm, but not demonstrated theoretically [49]. Thus, an initial benchmark for assessment of NES performance can be set at this limit for the oscillatory contribution at the dominant 1.5 EO for a 3-cylinder engine. Parametric simulations are carried out using the above mentioned range of parameters for J_N, k_N and c_N in the drivetrain model equipped with a single NES, attached to the clutch disc. A transient manoeuvre in 1st gear at 25% throttle is carried out. The data obtained is presented in the form of a contour plot, displaying the area where reduction of acceleration amplitude is achieved.

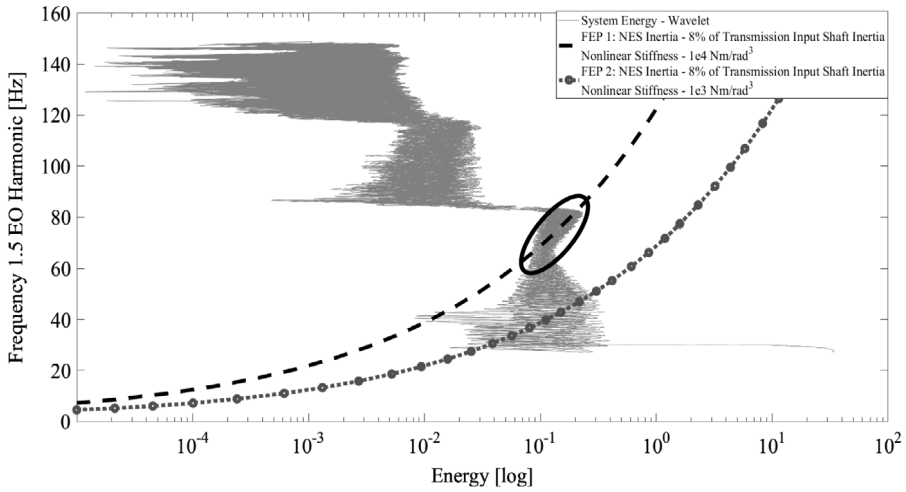

Fig. 9. FEP of the drivetrain model equipped with a single cubic NES, targeting a low frequency range (1st gear engaged at 25% throttle).

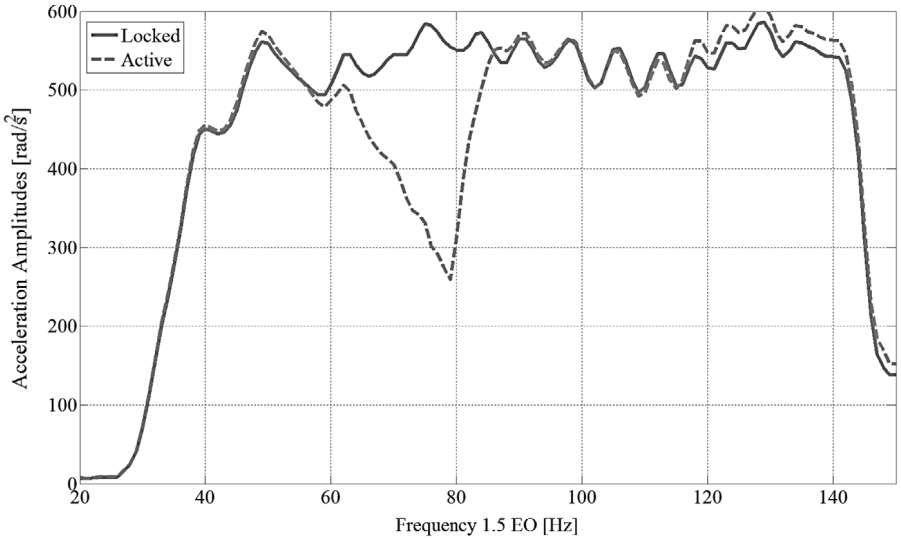

Fig. 10. Acceleration amplitude contribution at 1.5 EO at the transmission input shaft 1st gear engaged at 25% throttle) for a drivetrain equipped with a single NES (J_N = 8% of the transmission input shaft inertia, $k_N = 1 \times 10^4$ Nm/rad^3, c_N = 0.001 Nms/rad).

A second criterion to evaluate the NES performance is the Area of Effective Acceleration Amplitude Reduction (AEAAR), calculated using the trapezoidal rule to determine the areas under the acceleration amplitude curve during the transient manoeuvre for models with *active* and *locked* NES (Fig. 11). The difference between these areas provides the AEAAR highlighted by the shaded area in the figure, as:

$$Area = trapz\left(F_L, A_L\right) - trapz\left(F_A, A_A\right) \tag{13}$$

where:

$F_L = 1.5EO$ frequency of the *locked* system

$A_L =$ Acceleration amplitudes of the *locked* system

$F_A = 1.5EO$ frequency of the *active* system

$A_A =$ Acceleration amplitude of the *active* system

The simulation results are shown in the contour plot of Fig. 12, where the x-axis signifies variations of NES inertia and y-axis is the variation in the NES restoring force coefficient. The colour bar on the right-hand side of the plot signifies the AEAAR index. As expected, the higher the AEAAR index, the larger is the reduction in the acceleration amplitude. Fig. 12 shows that there is a range of NES restoring force coefficient and inertia which provides for effective NES performance. A randomly chosen point from the contour plot (indicated by the solid line circle) is initially selected and the corresponding acceleration amplitude plot is

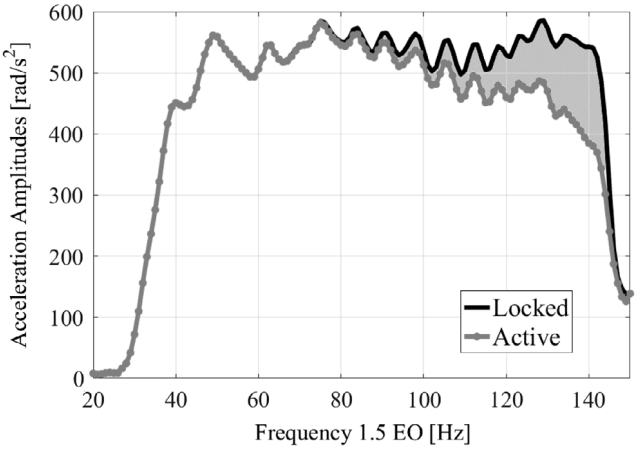

Fig. 11. Quantification of the Area of Effective Acceleration Amplitude Reduction.

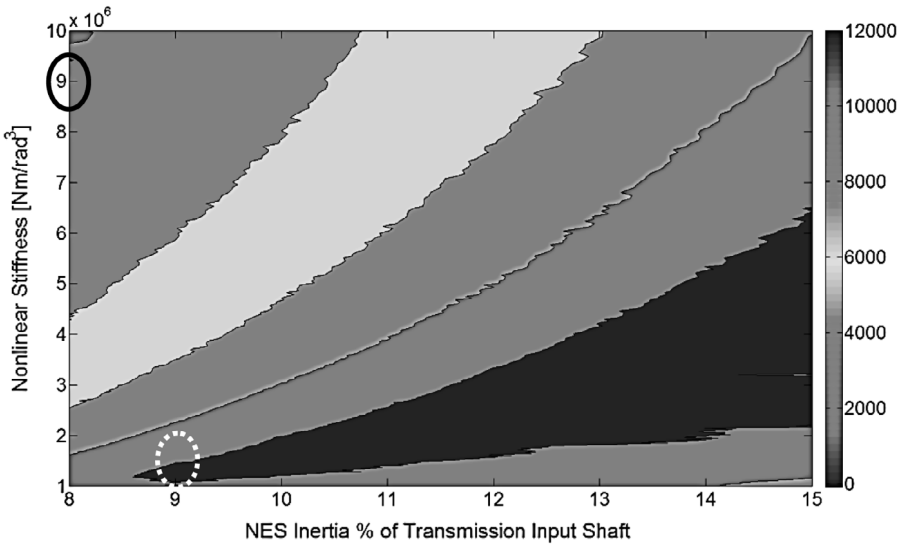

Fig. 12. Area of Effective Acceleration Amplitude Reduction (AEAAR) of the transmission input shaft for a drivetrain with a single NES (1st gear engaged at 25% throttle).

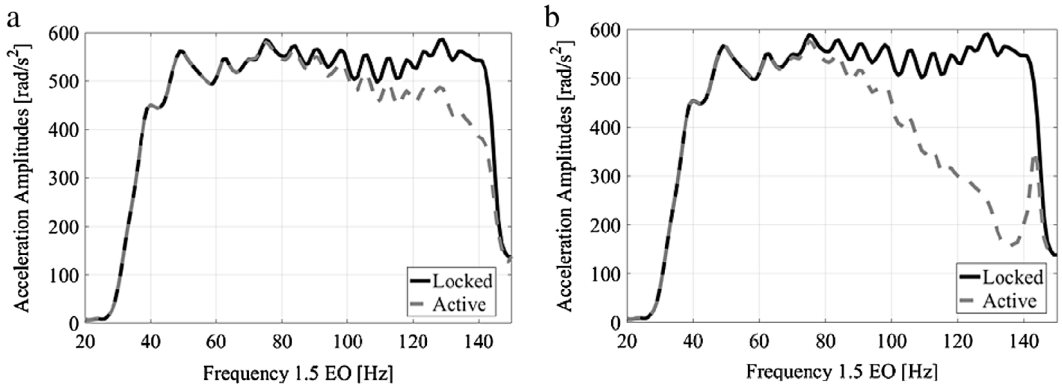

Fig. 13. a) Acceleration amplitude of the 1.5 EO contribution at the transmission input shaft (J_N = 8% of the transmission input shaft inertia, $k_N = 9\times10^6$ Nm/rad^3, c_N = 0.001 Nms/rad) and b) Acceleration amplitudes of the 1.5 EO contribution at the transmission input shaft (NES with optimised parameters J_N = 9% of the transmission input shaft inertia, $k_N = 1.2\times10^6$ Nm/rad^3, c_N = 0.001 Nms/rad).

shown in Fig. 13(a). The NES parameters corresponding to this plot are: *J_N = 8% of the transmission input shaft inertia, $k_N = 9\times10^6$ Nm/rad^3 and c_N = 0.001 Nms/rad* which result in an AEAAR of 4000 rad/s^3, representing jerk. The reduced acceleration amplitude *da* for a narrow increment of engine speed, represented by a frequency increment *df* is represented by the incremental reduction area: *-dAdf*. Therefore, for a frequency band, Δf the AEAAR becomes:

$$\text{AEAAR} = -\iint dA\,df = -\iint dA\,df\frac{dt}{dt} = -\iint \frac{dA}{dt}df\,dt = -\Delta f\int \dot{A}dt \tag{14}$$

where, $\dot{A}$ is the angular jerk in units of rad/s^3.

As it can be seen from the acceleration amplitudes and the corresponding time history plot in Fig. 14, for these combination of parameters the NES does not provide any significant benefit, when compared with the *locked* NES response.

As low NES inertia is desired in automotive applications, with maximisation AEAAR as a measure of effective NES performance, the following set of NES characteristics is chosen for a study: *J_N = 9% of transmission input shaft inertia, $k_N = 1.2\times10^6$ Nm/rad^3* and *c_N = 0.001 Nms/rad*. These characteristics correspond approximately to an AEAAR value of 12000 rad/s^3 in the contour plot of Fig. 12 (dash-line circle). The 1.5 EO acceleration amplitudes for the transient manoeuvre generated by this NES are shown in Fig. 13(b), clearly indicating a significant vibration attenuation (at frequencies above 80 Hz) when compared with the previously examined case. From the presented results it can be concluded that an increase in AEAAR has a direct effect on the amplitude reduction at the 1.5 EO.

The time history of the transmission input shaft angular velocity for the NES exhibiting higher AEAAR is shown in Fig. 15. The frequency range where this NES configuration suppresses the oscillations at 1.5 EO is approximately 80–140 Hz, accounting for almost 50% of the frequency range in the drivetrain's manoeuvre (with the engine speed ranging between 3300–5500 rpm). The reduction of the input shaft oscillations is initiated at approximately 3s, where a slight shift can be noted between the *locked* and *active* NES performances. In the inset to Fig. 15 around 7s, the angular velocity fluctuations for the system with an *active* NES are considerably reduced when compared with the system with a *locked* NES. This accounts for a significant reduction at the 1.5 EO amplitude contribution (Fig. 13(b)). A similar effect can be observed in the time history of the transmission input shaft angular velocity, where the rigid body mode is eliminated (Fig. 16). It is evident that the reduction in the amplitude of oscillations initiates after 3s (with a substantial reduction noted between 6 and 7s). Moreover, no negative effect was observed due to the NES action on EO multiples (e.g. 3.0, 4.5 EO) and transient manoeuvres/engaged gears/throttle levels. The 1.5 EO acceleration amplitudes depicting the effective performance of the NES for the 2nd gear engaged at 25% throttle transient manoeuvre are shown in Fig. 17.

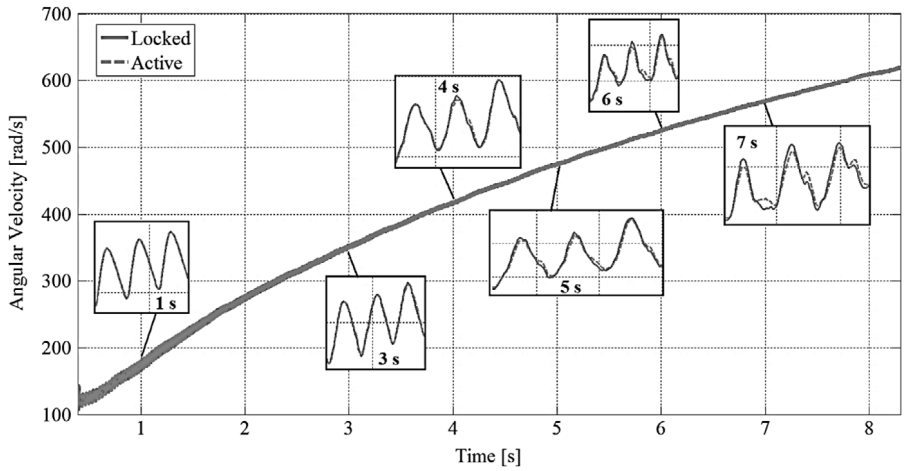

Fig. 14. Angular velocity of the transmission input shaft for cases with *active* and *locked* NES (J_N = 8% of the transmission input shaft inertia, $k_N = 9\times10^6$ Nm/rad^3, c_N = 0.001 Nms/rad).

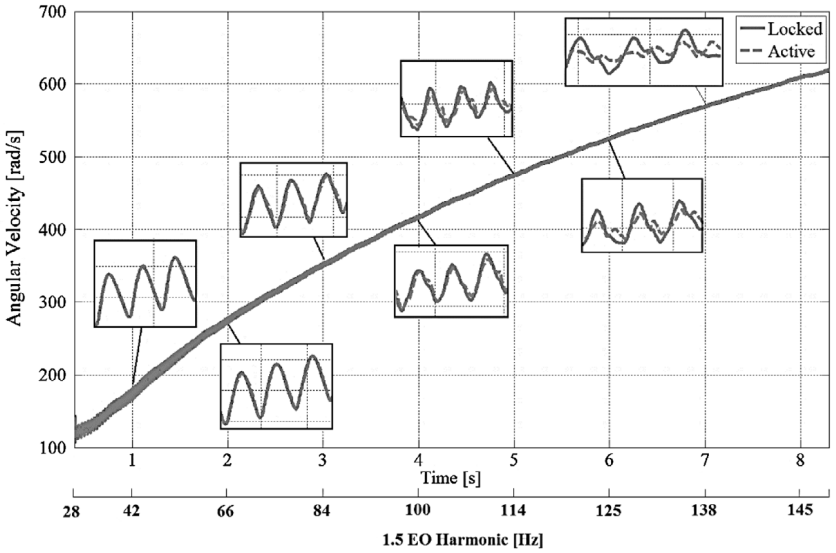

Fig. 15. Angular velocity time history of the transmission input shaft with *active* and *locked* NES (J_N = 9% of the transmission input shaft inertia, $k_N = 1.2\times10^6$ Nm/rad^3, c_N = 0.001 Nms/rad).

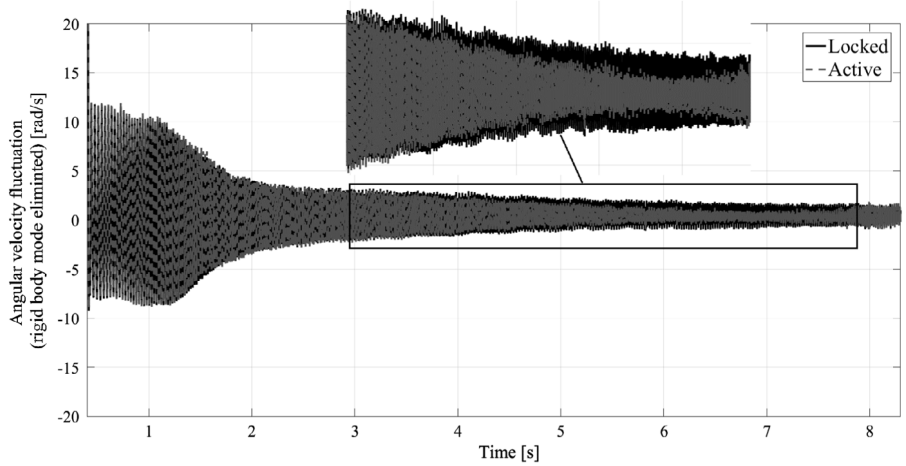

Fig. 16. Transmission input shaft velocity time history with the rigid body mode eliminated (1st gear engaged at 25% throttle).

An FEP plot is produced to interpret the presented results. This is shown in Fig. 18, including the backbone curve of the NNM motion of the NES with the superposition of the energy (wavelet) of the drivetrain model. It can be seen that the effectiveness of the NES is governed by

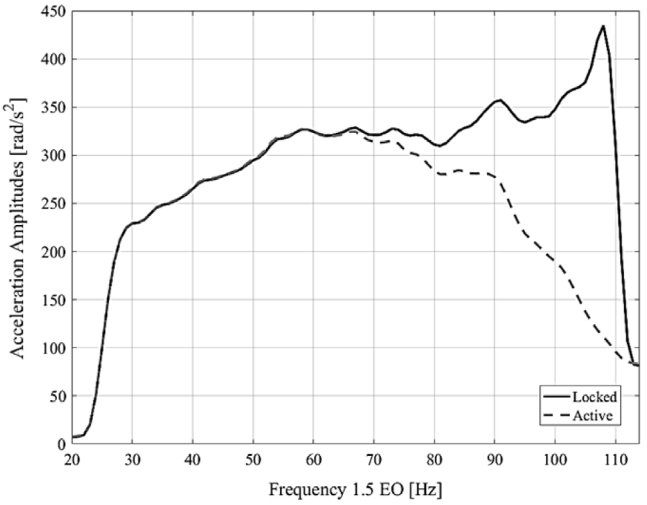

Fig. 17. Acceleration amplitudes of the 1.5 EO contribution at the transmission input shaft for 2nd gear engaged at 25% throttle (J_N = 9% of the transmission input shaft inertia, k_N = 1.2×10^6 Nm/rad^3, c_N = 0.001 Nms/rad).

the applied input energy. Furthermore, the frequency range of the NES 1.5 EO acceleration amplitude reduction (Fig. 13(b)) matches well with the frequency range (80–140 Hz) in the FEP plot, where the backbone curve overlaps with the energy wavelet results.

4. Powertrain coupled with 2 parallel NES

The analyses presented thus far concern the effect of a single cubic NES in an automotive drivetrain for attenuating engine order oscillations. The results obtained demonstrate that significant vibration attenuation can be achieved over a broad frequency range, primarily evident towards the higher end of the studied spectrum (80–140 Hz). Since drivetrain operating conditions also concern lower frequency ranges of excitation (below 80 Hz), it is important to explore the effect of incorporating a second NES in order to target this frequency range as well. The aim is to tune the second NES for attenuating oscillations below 80 Hz in a complementary manner to the already deployed NES (Fig. 13(b)). The reduced order drivetrain model with the incorporation of this second NES is shown in Fig. 19. The matrix formulation for the above model with an *active* NES (Eq. (15)) and *locked* NES (Eq. (16)) becomes:

$$[\boldsymbol{J}]\begin{bmatrix}\ddot{\theta}_2\\ \ddot{\theta}_3\\ \ddot{\theta}_{N1}\\ \ddot{\theta}_{N2}\end{bmatrix}+[\boldsymbol{C_N}]\begin{bmatrix}\dot{\theta}_2\\ \dot{\theta}_3\\ \dot{\theta}_{N1}\\ \dot{\theta}_{N2}\end{bmatrix}+[\boldsymbol{K}]\begin{bmatrix}\theta_2\\ \theta_3\\ \theta_{N1}\\ \theta_{N2}\end{bmatrix}=\begin{bmatrix}k_1\theta_F+c_1\dot{\theta}_F-k_{N1}(\theta_2-\theta_{N1})^3-k_{N2}(\theta_2-\theta_{N2})^3\\ -T_{Res}\\ k_{N1}(\theta_2-\theta_{N1})^3\\ k_{N2}(\theta_2-\theta_{N2})^3\end{bmatrix} \tag{15}$$

where:

$$[\boldsymbol{J}]=\begin{bmatrix}J_2&0&0&0\\0&J_3&0&0\\0&0&J_{N1}&0\\0&0&0&J_{N2}\end{bmatrix},[\boldsymbol{K}]=\begin{bmatrix}k_1+k_2&-k_2&0&0\\-k_2&k_2&0&0\\0&0&0&0\\0&0&0&0\end{bmatrix},$$

$$[\boldsymbol{C_N}]=\begin{bmatrix}c_{(1,1)}&c_{(1,2)}&-c_{N1}&-c_{N2}\\c_{(2,1)}&c_{(2,2)}&0&0\\-c_{N1}&0&c_{N1}&0\\-c_{N2}&0&0&c_{N2}\end{bmatrix}$$

$$\begin{bmatrix}J2+J_{N1}+J_{N2}&0\\0&J_3\end{bmatrix}\begin{bmatrix}\ddot{\theta}_2\\ \ddot{\theta}_3\end{bmatrix}+[\boldsymbol{C}]\begin{bmatrix}c\dot{\theta}_2\\ \dot{\theta}_3\end{bmatrix}+\begin{bmatrix}cck_2+k_1&-k_2\\-k_2&k_2\end{bmatrix}\times\begin{bmatrix}c\theta_2\\ \theta_3\end{bmatrix}=\begin{bmatrix}ck_1\theta_F+c_1\dot{\theta}_F\\ -T_{Res}\end{bmatrix}. \tag{16}$$

The same methodology as before, producing FEP plots to obtain the range of NES parameters is used for the frequency range: 50–80 Hz, whilst ensuring synergistic operation with the previous NES attachment. The FEP plot for the NES targeting lower frequencies is shown in Fig. 20. The NES tuned at low frequencies induces energy redistribution in the primary system, particularly notable at higher frequencies (90–140 Hz) with severe energy fluctuations (10^{-4} – 10^{-2}). In contrast, in the FEP of Fig. 16 (NES tuned to the higher frequencies) the converse is evident (energy fluctuations are higher at low frequencies). This energy redistribution is a main feature of the effective TET and NES operations.

Using the above FEP analysis, it is clear that a promising range for the restoring force coefficient targeting low frequencies is k_N = 2×10^3 – 2×10^4 *Nm/rad*^{3}. The NES inertia range is chosen with the objective of keeping it as low as possible (J_N = *2 –10%* of the transmission input shaft inertia) and the damping coefficient as in the previous case is c_N = *0.001 Nms/rad*. Following an extensive set of numerical

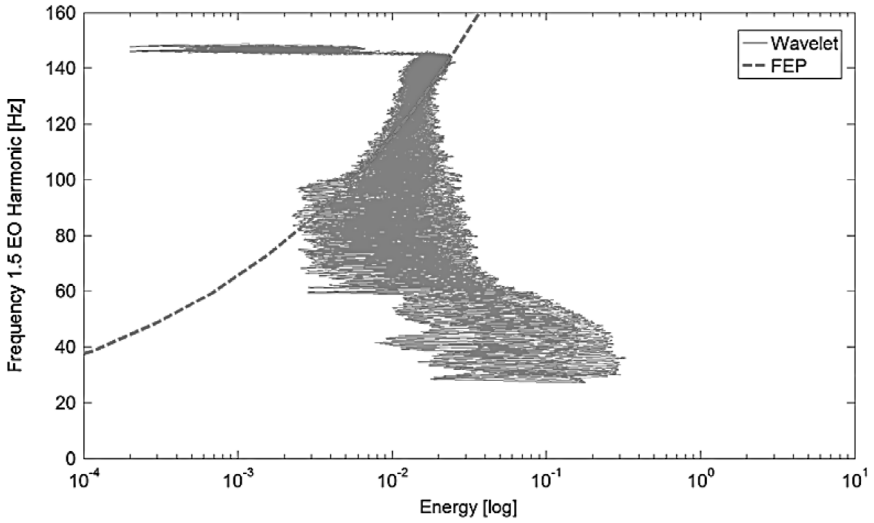

Fig. 18. FEP of the single NES exhibiting high AEAAR with superposition of the 1.5 EO wavelet, targeting a high frequency range (1st gear engaged at 25% throttle).

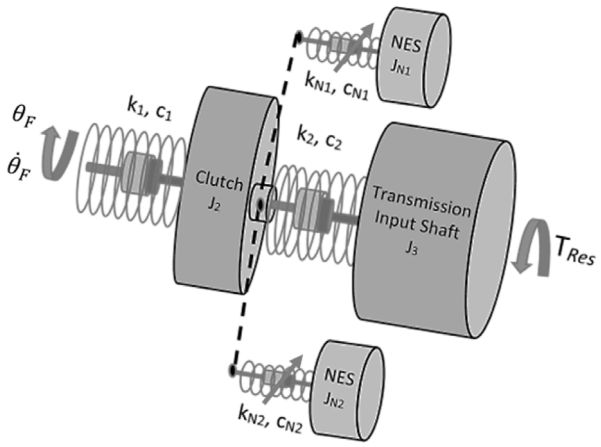

Fig. 19. Schematic representation of the drivetrain model equipped with 2 parallel NES.

simulations, employing the transient manoeuvre at 1st gear engaged with 25% throttle, a contour plot is generated showing the AEAAR for different NES characteristics (Fig. 21).

The contour plot of Fig. 21 shows that when using appropriate NES parameter combinations, significant reduction in oscillations can be achieved. The NES parameter combination inducing the best performance is $J_N = 7\%$ *of the transmission input shaft inertia,* $k_N = 0.2 \times 10^4$ *Nm/rad*^{3} *and* $c_N = 0.001$ *Nms/rad,* leading to an AEAAR value of 2000 rad/s^3 (circled region). The corresponding 1.5 EO acceleration amplitudes of the input shaft are shown in Fig. 22. It can be observed that acceleration reduction is achieved in the frequency range 50–75 Hz (corresponding to the engine speed range of: 1980–3000 rpm.). The same effect can be seen in the time history of Fig. 23 with the inset plot at 2s, demonstrating the corresponding vibration attenuation.

The synergistic effect of the two NESs, acting in parallel, results in the reduction of the 1.5 EO contribution over a wider frequency range (Fig. 24). The characteristics of the two NESs are: low-frequency operating NES with $J_{N1} = 7\%$ *of transmission input shaft inertia,* $k_{N1} = 0.2 \times 10^4$ *Nm/rad*^{3} and $c_{N1} = 0.001$ *Nms/rad* and high-frequency operating NES with $J_{N2} = 9\%$ *of transmission input shaft inertia,* $k_{N2} = 1.2 \times 10^6$ *Nm/rad*^{3} and $c_{N2} = 0.001$ *Nms/rad.* As a result, the frequency range of vibration attenuation is 55–145 Hz. This observation signifies that implementing the two NESs with a combined inertia of 16% of the transmission input shaft inertia would result in reduction of vibration for the wider range of engine speed: 1980–5500 rpm. The synergistic behaviour of the two parallel NESs can also be observed in the time history of the transmission input shaft velocity fluctuations of Fig. 25 (with the rigid body mode eliminated).

The effect of the two parallel NESs on the 1.5 EO acceleration amplitudes of the transmission input shaft is demonstrated in both frequency and time domains. An FEP including the NNMs of both NESs is shown in Fig. 26. The graph exhibits the frequency region of vibration attenuation for each of the two NESs (circled) with the inset to the figure showing the corresponding acceleration amplitude. The energy fluctuations at 1.5 EO (wavelet) are reduced significantly, when compared with the systems with a single NES attachment.

5. Conclusions

The new generations of engines incorporating technologies primarily aimed at fuel efficiency and reduced emissions can induce broadband, high amplitude torsional oscillations in the drivetrain systems. The effect of multiple NES absorbers on reduction of vibrations of an automotive drivetrain is studied. A methodology for selecting the characteristics of the NES is described. The absorbers are coupled to the clutch disc in order to reduce the severity of undesirable input EO oscillations. The presented study uses a reduced order linear dynamic model of an automotive drivetrain, validated in both frequency and time domains against experimental data obtained from a vehicle equipped with the same powertrain. Single and multiple NESs are coupled in parallel to the clutch disc of the drivetrain model and their effect on the reduction of broad band torsional oscillations is analysed. Through the use of FEP, a range of feasible NES parameters is selected with the objective of determining the optimal features of nonlinear absorber(s) for TET purposes over a suitably broad range of frequencies. The performance of the selected NES parameter combination is confirmed using time and frequency domain analyses. The synergistic action of two NES in parallel is demonstrated, showing that vibration suppression can be achieved over a wide range of frequencies. The advantage of this approach is the introduction of a relatively small increase in the overall drivetrain inertia.

The effective performance of the NES largely depends on the energy input into the system, which defines an operating threshold for the NES design. Following a successful experimental verification (as part of the future work), the implementation of NES in automotive drivetrains would have the potential of replacing some of the current palliative measures, for particularly troublesome NVH phenomena such as gear rattle and clutch in-cycle vibration, with reduced weight and package space requirements. Therefore, assessing the NES performance against other palliatives widely used in industry to reduce drivetrain oscillations is also part of the future work.

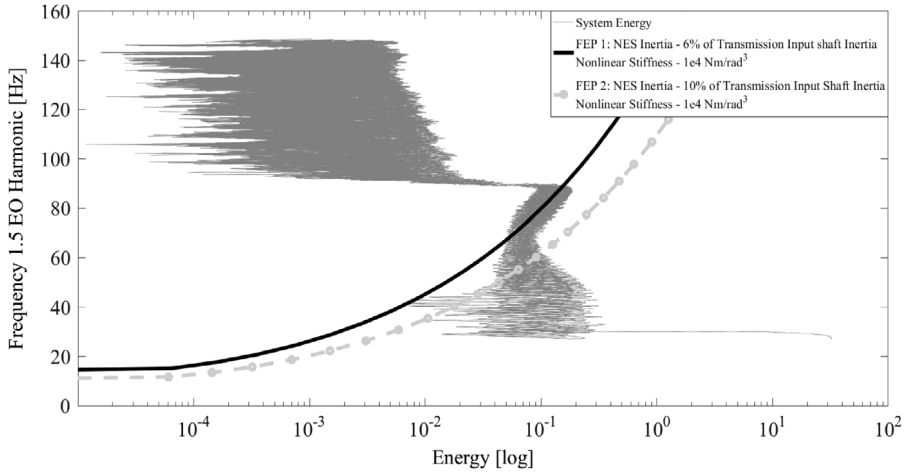

Fig. 20. FEP of the single DoF grounded NES targeting lower frequencies with superposition of the 1.5 EO wavelet.

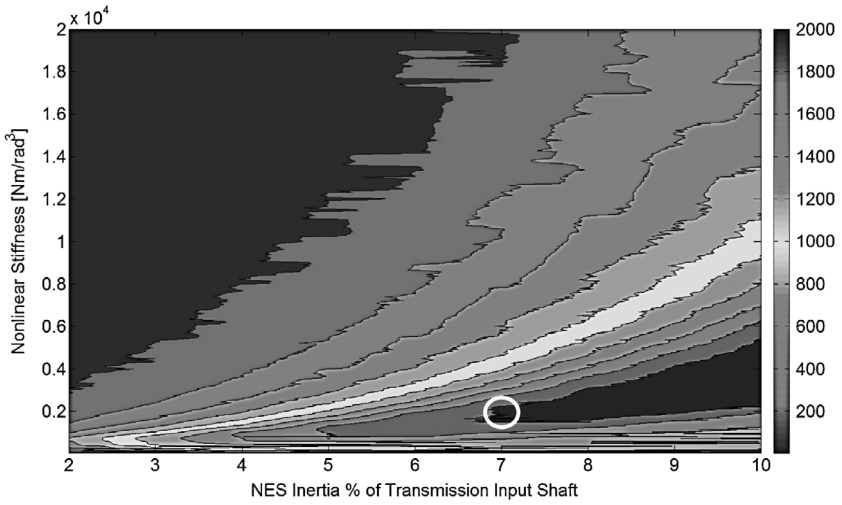

Fig. 21. Area of Effective Acceleration Amplitude Reduction of the transmission input shaft for the NES targeting lower frequencies (1st gear engaged at 25% throttle).

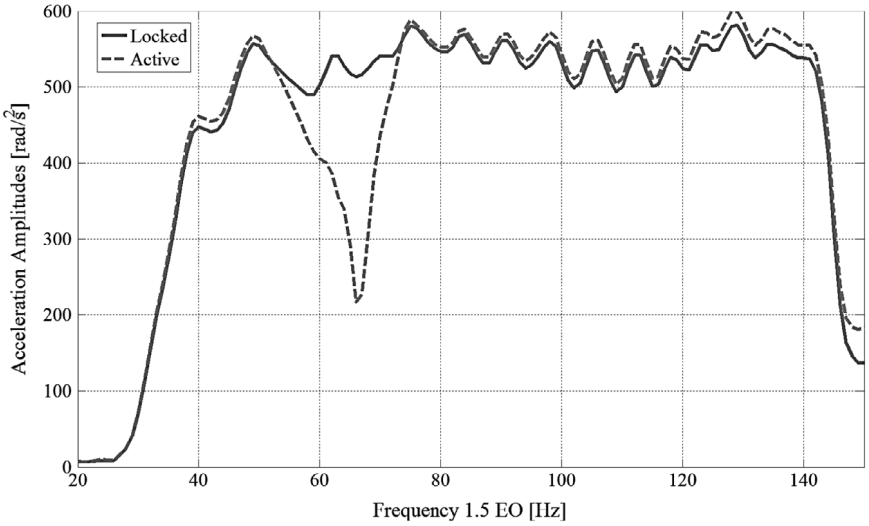

Fig. 22. Acceleration amplitudes of the 1.5 EO at the transmission input shaft for the NES targeting lower frequencies (J_N = 7% of transmission input shaft inertia, $k_N = 0.2 \times 10^4$ Nm/rad^3 and $c_N = 0.001$ Nms/rad).

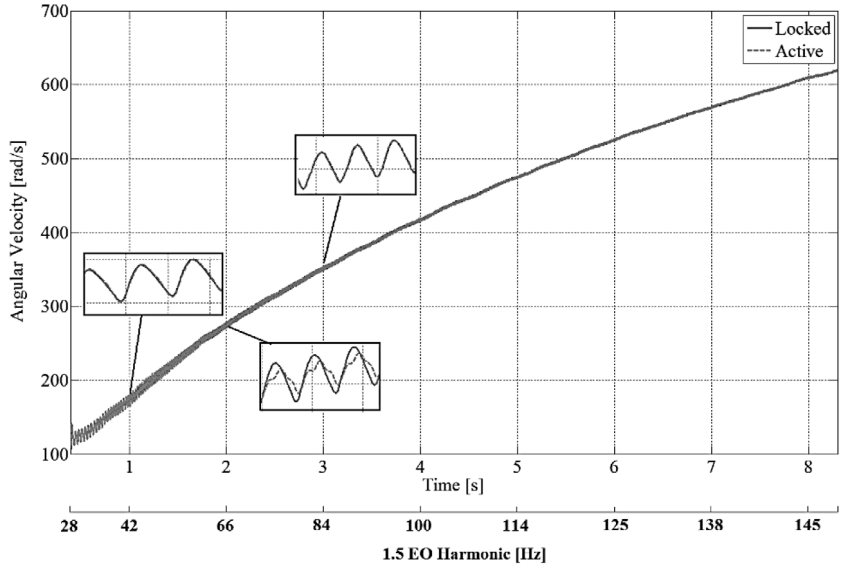

Fig. 23. Angular velocity time history of the transmission input shaft with *active* and *locked* NES targeting lower frequencies (J_N = 7% of transmission input shaft inertia, $k_N = 0.2 \times 10^4$ Nm/rad^3 and $c_N = 0.001$ Nms/rad).

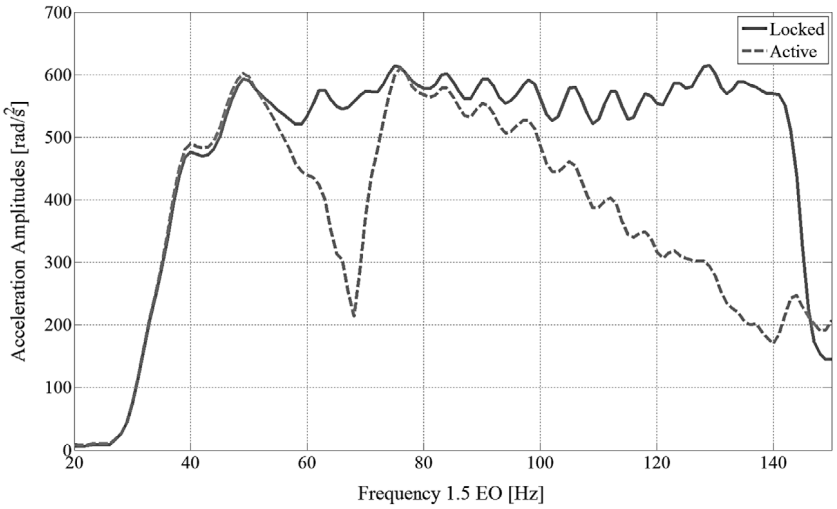

Fig. 24. Acceleration amplitude contribution at 1.5 EO at the transmission input shaft for the drivetrain model with two parallel NESs.

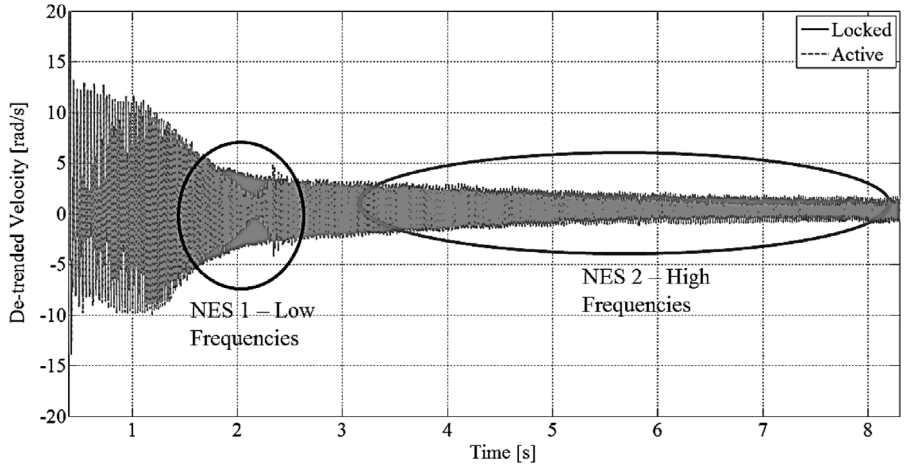

Fig. 25. Transmission input shaft velocity time history with the rigid body mode eliminated for a drivetrain with two parallel NESs acting (1st gear engaged at 25% throttle).

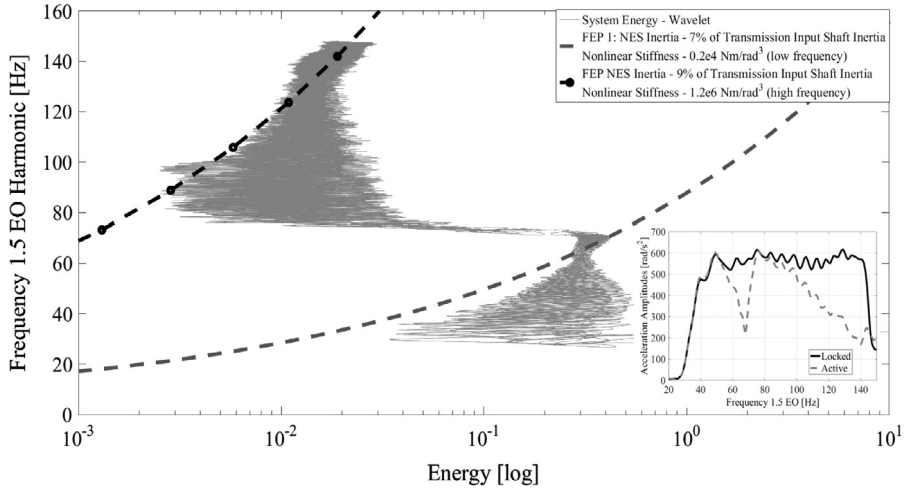

Fig. 26. FEP of the optimised parallel NES with superposition of the 1.5 EO (wavelet).

Acknowledgements

The authors wish to express their gratitude to the EPSRC for the financial support extended to the **"Targeted energy transfer in powertrains to reduce vibration-induced energy losses"** Grant (EP/L019426/1), under which this research was carried out. Thanks are also due to Raicam Clutch and Ford Motor Company for their technical support, as well as to Dr. Maxime Peeters for kindly providing the software to compute the NNMs. Research data for this paper are available on request from Stephanos Theodossiades.

References

[1] T. Hasebe, H. Yamamoto, K. Morita, K. Hibi, T. Ninomiya, Y. Goto, Experimental study of reduction methods for clutch pedal vibration and drive train rattling noise from clutch system, SAE Technical Paper, No. 932007, 1993.
[2] P. Kelly, H. Rahnejat, J.W. Biermann, C553/013/98: Multi-body dynamics investigation of clutch pedal in-cycle vibration (whoop), in: IMECHE Conference Transactions, 13, 1998, pp. 167–178.
[3] P. Kelly, M. Menday, H. Rahnejat, M. Ebrahimi, Powertrain refinement: A combined experimental and multi-body dynamics analysis approach, in: Proc. 8th Aachen Colloquium, Aachen, Germany, 1999, pp. 1079–1094.
[4] M.Y. Wang, R. Manoj, W. Zhao, Gear rattle modelling and analysis for automotive manual transmissions, Proc. IMechE, Part D: J. Automobile Eng. 215 (2) (2001) 241–258.
[5] O. Tangasawi, S. Theodossiades, H. Rahnejat, Lightly loaded lubricated impacts: Idle gear rattle, J. Sound Vib. 308 (3) (2007) 418–430.
[6] R. Russo, R. Brancati, E. Rocca, Experimental investigations about the influence of oil lubricant between teeth on the gear rattle phenomenon, J. Sound Vib. 321 (3) (2009) 647–661.
[7] M. De la Cruz, S. Theodossiades, H. Rahnejat, An investigation of manual transmission drive rattle, Proc. IMechE, Part K: J Multi-body Dyn 224 (2) (2010) 167–181.
[8] H. Rahnejat, Multi-Body Dynamics: Vehicles, Machines and Mechanisms, Professional Engineering Publishing, Bury St Edmunds, UK, 1998.
[9] A. Plötner, Ö. Bilen, F. Küçükay, Simulation of the drive-off performance with turbocharged diesel engines, IFAC Proc. 45 (30) (2012) 146–153.
[10] M. Pfabe, C. Woernle, Reducing torsional vibrations by means of a kinematically driven flywheel — Theory and experiment, Mech. Mach. Theory 102 (2016) 217–228.
[11] J.-S. Chen, H.-Y. Hwang, Engine automatic start-stop dynamic analysis and vibration reduction for a two-mode hybrid vehicle, Proc. IMechE, Part D: J. Automobile Eng. 227 (9) (2013) 1303–1312.
[12] S. Theodossiades, M. Gnanakumarr, H. Rahnejat, P. Kelly, Effect of a dual-mass flywheel on the impact-induced noise in vehicular powertrain systems, Proc. IMechE, Part D: J. Automobile Eng. 220 (6), (2006) pp. 747–761.
[13] P. Kelly, B. Pennec, R. Seebacher, B. Tlatlik, M. Mueller, Dual mass flywheel as a means of attenuating rattle, in: Tribology and Dynamics of Engine and Powertrain: Fundamentals, Applications and Future Trends, 2010, pp. 857–877.
[14] A.S. Alsuwaiyan, S.W. Shaw, Performance and dynamic stability of general-path centrifugal pendulum vibration absorbers, J. Sound Vib. 252 (5) (2002) 791–815.
[15] D.E. Newland, Nonlinear aspects of the performance of centrifugal pendulum vibration absorbers, ASME J. Manuf. Sci. Eng. 86 (1964) 257–263.
[16] P. Bertin, E. Breton, A. Mokdad, Radial Dual Mass Flywheel, SAE Tech. Pap. 950893, 1995.
[17] D. Chen, Y. Ma, W. Sun, X. Guo, X. Shi, Research of design and vibration reduction of dual mass flywheel with arc helix spring, in: Proc. Int. Conf. on Electronic & Mech. Eng. and Info. Tech., 5, 2011, pp. 2706–2709.
[18] H. Rahnejat, S. Theodossiades, P. Kelly, M.T. Menday, Drivetrain noise, vibration, and harshness, in: Encyclopedia of Automotive Engineering, John Wiley, 2014.
[19] P. Kelly, H. Rahnejat, Clutch pedal dynamic noise and vibration investigation, in: Multi-body Dynamics: Monitoring and Simulation Techniques, MEP, Bury St Edmunds, 1997.
[20] D. Arrundale, S. Gupta, H. Rahnejat, Multi-body dynamics for the assessment of engine induced inertial imbalance and torsional–deflection vibration, in: Multi-Body Dynamics: Monitoring and Simulation Techniques II, Professional Engineering Publishing, 2000, pp. 207–232.
[21] R.A. Krenz, 1985 Vehicle response to throttle tip-in/tip-out, SAE Technical Paper, No. 850967.
[22] M.T. Menday, H. Rahnejat, M. Ebrahimi, Clonk: An onomatopoeic response in torsional impact of automotive drivelines, Proc. IMechE, Part D: J. Automobile Eng. 213 (4) (1999) 349–357.
[23] S. Theodossiades, M. Gnanakumarr, H. Rahnejat, M. Menday, Mode identification in impact-induced high-frequency vehicular driveline vibrations using an elasto-multi-body dynamics approach, Proc. IMechE. Part K: J Multi-body Dyn. 218 (2) (2004) 81–94.
[24] A. Vakakis, O.V. Gendelman, L.A. Bergman, D.M. McFarland, G. Kerschen, Y.S. Lee, Nonlinear Targeted Energy Transfer in Mechanical and Structural Systems: Solid Mechanics and Its Applications, first ed., Springer, 2008.
[25] A.F. Vakakis, O. Gendelman, Energy pumping in nonlinear mechanical oscillators: Part II—resonance capture, J. Appl. Mech. 68 (2001) 42–48.
[26] O. Gendelman, L.I. Manevitch, A.F. Vakakis, R. M'Closkey, Energy pumping in nonlinear mechanical oscillators: Part I—dynamics of the underlying hamiltonian systems, J Appl. Mech. 68 (2001) 34.
[27] A.F. Vakakis, L.I. Manevitch, O. Gendelman, L. Bergman, Dynamics of linear discrete systems connected to local, essentially non-linear attachments, J. Sound Vib. 264 (2003) 559–577.
[28] X.. Jiang, D.M. Mcfarland, L.A. Bergman, A.F. Vakakis, Steady state passive nonlinear energy pumping in coupled oscillators: Theoretical and experimental results, Nonlinear Dynam. 33 (2003) 87–102.
[29] P.N. Panagopoulos, A.F. Vakakis, S. Tsakirtzis, Transient resonant interactions of finite linear chains with essentially nonlinear end attachments leading to passive energy pumping, Int. J. Solids Struct. 41 (2004) 6505–6528.
[30] D.M. McFarland, L.A. Bergman, A.F. Vakakis, Experimental study of non-linear energy pumping occurring at a single fast frequency, Int. J. Non. Linear. Mech. 46 (2005) 891–899.
[31] G. Kerschen, Y.S. Lee, A.F. Vakakis, D.M. McFarland, L.A. Bergman, Irreversible passive energy transfer in coupled oscillators with essential nonlinearity, SIAM J. Appl. Math. 66 (2) (2005) 648–679.
[32] Y.S. Lee, G. Kerschen, A.F. Vakakis, P. Panagopoulos, L. Bergman, D.M. McFarland, Complicated dynamics of a linear oscillator with a light, essentially nonlinear attachment, Phys. D Nonlinear Phenom. 204 (2005) 41–69.
[33] F. Georgiadis, A.F. Vakakis, D.M. Mcfarland, L. Bergman, Shock isolation through passive energy pumping caused by nonsmooth nonlinearities, Int. J. Bifurc. Chaos 15 (6) (2005) 1989–2001.
[34] O.V. Gendelman, T. Sapsis, A.F. Vakakis, L.A. Bergman, Enhanced passive targeted energy transfer in strongly nonlinear mechanical oscillators, J. Sound Vib. 330 (1) (2011) 1–8.
[35] N.E. Wierschem, D.D. Quinn, S.A. Hubbard, M.A. Al-Shudeifat, D.M. McFarland, J. Luo, L.A. Fahnestock, B.F. Spencer, A.F. Vakakis, L.A. Bergman, Passive damping enhancement of a two-degree-of-freedom system through a strongly nonlinear two-degree-of-freedom attachment, J. Sound Vib. 331 (25) (2012) 5393–5407.
[36] R. Viguié, G. Kerschen, J.C. Golinval, D.M. McFarland, L.A. Bergman, A.F. Vakakis, N. Van de Wouw, Using passive nonlinear targeted energy transfer to stabilize drill-string systems, Mech. Syst. Signal Process. 23 (2009) 148–169.
[37] D. Centea, H. Rahnejat, M.T. Menday, Non-linear multi-body dynamic analysis for the study of clutch torsional vibrations (judder), Appl. Math. Model. 25 (3) (2001) 177–192.
[38] D. Centea, H. Rahnejat, M.T. Menday, The influence of the interface coefficient of friction upon the propensity to judder in automotive clutches, Proc. IMechE, Part D: J. Automobile Eng. 213 (3) (1999) 245–258.
[39] E.M. Rabeih, D.A Crolla, Intelligent control of clutch judder and shunt phenomena in vehicle drivelines, Int. J. Vehicle Des. 17 (3) (1996) 318–332.
[40] A. Haris, E. Motato, S. Theodossiades, A.F. Vakakis, L.A. Bergman, D.M. McFarland, B. Struve, Targeted Energy Transfer in Automotive Powertrains, Proc. Dynamics Systems: Mathematical and Numerical Approaches, Poland, 2015, pp. 245–254.
[41] B. Mashadi, D.A. Crolla, Vehicle Longitudinal Dynamics, in: Vehicle Powertrain Systems, Wiley, 2012, pp. 133–135.
[42] T.K. Caughey, M.E.J. O'Kelly, Classical normal modes in damped linear dynamic systems (classical normal modes in discrete and continuous viscously damped linear dynamic systems), J. Appl. Mech. 32 (6) (1965) 583–588.
[43] G. Scagliarini, R. Viguié, G. Kerschen, F. Pellicano, Spur Gear Vibration Mitigation by Means of Energy Pumping. In: Proceedings of the IMAC-XXVII Florida, USA, 2009.
[44] N.E. Wierschem, M.A. AL-Shudeifat, B.F. Spencer, . JR, A.F. Vakakis, L.A. Bergman, 2014. Experimental investigation of a rotational nonlinear energy sink for shock mitigation, Proceedings of the ASME Design Engineering Technical Conference 2014.
[45] F. Petit, M. Loccufier, D. Aeyels, The energy thresholds of nonlinear vibration absorbers, Nonlinear Dynam. 74 (2013) 755–767.
[46] G. Kerschen, M. Peeters, J.C. Golinval, A.F. Vakakis, Nonlinear normal modes, part I: A useful framework for the structural dynamicist, Mech. Syst. Signal Process. 23 (2009) 170–194.
[47] M. Peeters, R. Viguié, G. Sérandour, G. Kerschen, J.C. Golinval, Nonlinear normal modes, part II: Toward a practical computation using numerical continuation techniques, Mech. Syst. Signal Process. 23 (2009) 195–216.
[48] E. Motato, A. Haris, S. Theodossiades, M. Mohammadpour, H. Rahnejat, P. Kelly, A.F. Vakakis, D.M. McFarland, L.A. Bergman, Targeted energy transfer and modal energy redistribution in automotive drivetrains, Nonlinear Dynam. 87 (1) (2016) 1–22.
[49] A. Kooy, in: Schaeffler Technologies GmbH & Co (Ed.), Isolation Is the Key, in: Solving the Powertrain Puzzle, Springer Fachmedien Wiesbaden, 2014, pp. 78–93.